# Generalization of interlayer tunneling models to cuprate superconductors with charge density waves

Hércules Santana and E. V. L. de Mello [*]

*Instituto de Física, Universidade Federal Fluminense, 24210-346 Niterói, Rio de Janeiro, Brazil*

Since the discovery of cuprate superconductors, the interlayer tunneling (ILT) and Lawrence-Doniach (LD) models, which connect CuO planes by Josephson coupling, were considered the leading theoretical proposals for these materials. However, measurements of the interlayer magnetic penetration depth $\lambda_c$ yielded larger values than required by the ILT model. After the discovery of planar stripes and incommensurate charge ordering, it was also possible to consider Josephson coupling between these mesoscopic charge domains or blocks. We show that the average intralayer is larger than the interlayer coupling and is comparable with the condensation energy, leading to a superconducting transition by long-range phase order. Another consequence is that the ratio $[\lambda_c/\lambda_{ab}]^2$ is related to the resistivity ratio $\rho_c/\rho_{ab}$ near the superconducting transition temperature, in agreement with several measurements.

## I. INTRODUCTION

Several experiments on high-temperature cuprate superconductors (HTS) verified their large anisotropic properties that arise mainly because of a much smaller resistivity ($\rho_{ab}$) along with the CuO layers. These facts suggested that the interlayer tunneling (ILT) [1–5] or Lawrence-Doniach (LD) models [6], which describe a layered superconductor as a stack of Josephson-coupled adjacent blocks or layers, were ideal candidates to describe the HTS. The ILT model of Anderson and collaborators [3,4] consisted of non-Fermi-liquid planar electrons and, in the superconducting (SC) phase, interlayer tunneling of Cooper pairs. This approach results in a strong decrease of the $c$-axis kinetic energy with a concomitant increase of the condensation energy (the gain of free energy in the SC state compared with the normal state).

On the experimental side, Shibauchi *et al.* [7] measured the magnetic penetration depth $\lambda_c$ and the planar $\lambda_{ab}$ in single crystals of La$_{2-x}$Sr$_x$CuO$_4$ (LSCO) and found that $\lambda_c(T)$ was in good agreement with the LD model. However, images of interlayer Josephson vortices [8] in single-layer compounds Tl$_2$Ba$_2$CuO$_6$ yielded about 20 µm, which is about 20 times the penetration depth determined by the ILT model [5]. This result was considered strong evidence against the ILT and LD models to cuprates [8,9] and they were abandoned as the leading general HTS theories.

On the other hand, over the years, a significant number of new experiments with novel techniques and methods revealed properties not known when the ILT was originally proposed, which opened new possibilities: In particular, charge inhomogeneities in the form of stripes were discovered in underdoped Nd substituted in LSCO by neutron scattering [10], which was a key experiment for the detection of charge-ordering (CO) or charge density wave (CDW)

phenomena in HTS. Along this line, scanning tunneling microscopy (STM) experiments made it possible to obtain atomically resolved maps [11,12] of the energy-dependent local density of states (LDOS). More recently, resonant x-ray diffraction (RXRD) revealed the subtle variations of the CO wavelength $\lambda_{CO}$ with the doping level of several families of cuprates [13].

To interpret their inhomogeneous STM data on underdoped Bi$_2$Sr$_2$CaCu$_2$O$_{8+\delta}$ (Bi2212), Lang *et al.* [11] proposed a structure of mesoscopic superconductor grains connected by Josephson coupling. This original proposal was not generally accepted, mainly because there was no evidence of CO instability near the optimal and in the overdoped region. However, a few years later, similar CO granular patterns were observed by STM near the optimal value [14] and even in the overdoped regions [15–17]. Furthermore, a variety of complementary experimental probes detected charge instability in all hole-doped HTS families [13] as well as in Nd-based electron-doped ones [18]. Recently, charge inhomogeneities have been detected in overdoped LSCO up to at least $x = p = 0.21$ [19–21] and possibly up to $p = 0.25$ [22]. Therefore, the ubiquitous presence of CDW in all HTS compounds suggested that they are intertwined with the SC phase and somehow related to the SC interaction [23–26].

To understand how they intertwine we use the Cahn-Hilliard (CH) equation that can simulate the observed CO wavelength $\lambda_{CO}$ of different materials employing a phase separation Ginzburg-Landau (GL) free energy. The $V_{GL}$ free energy can be tuned in different forms or shapes and acts as a template for the CO or CDW while confining the charges in alternating hole-rich and hole-poor domains. $V_{GL}$ works as a surface potential that binds the electrons in physical grains of a granular superconductor with the difference that the CDW domains are of nanoscopic dimensions. But the Cooper pair coherence lengths in HTS are also of nanoscopic sizes, and they may be formed by local hole pair interactions mediated by $V_{GL}$ modulations.

*Corresponding author: evlmello@id.uff.br

In this scenario, we calculate local SC amplitudes by a self-consistent Bogoliubov–de Gennes (BdG) approach. Akin to granular superconductors, there are Josephson couplings between the nanoscopic charge domains that compete with thermal disorder to promote long-range phase order at the SC critical temperature $T_c$ [26,27]. We also consider the planar Josephson coupling between the CO domains together with interlayer coupling to formulate a generalization of the ILT and LD models.

We mentioned above that the measurements and calculations of the penetration depth $\lambda_c$ were important tests of the ILT theories. On the other hand, the Josephson couplings are proportional to the local superfluid densities [28] that in turn are proportional to the inverse of the magnetic penetration depth [29], which is our route to estimate $\lambda_c$ and $\lambda_{ab}$. Using the LSCO calculations from Ref. [26] we reproduce several low-temperature $[\lambda_c(p)/\lambda_{ab}(p)]^2$ measurements [7,30]. We also demonstrate an equation relating this ratio to the resistivities $R_n^c/R_n^{ab}$ just above the SC transition, which is easy to test experimentally and is in agreement with several old measurements [31,32].

## II. CDW CALCULATIONS

We mentioned that the CH phase separation method reproduces the observed planar CDW, but its great advantage is the GL free-energy map that provides a scale to the pairing attraction. The starting point is the time-dependent phase separation order parameter associated with the relative local electronic density, $u(\mathbf{r}, t) = [p(\mathbf{r}, t) - p]/p$, where $p(\mathbf{r}, t)$ is the local charge or hole density at a position $\mathbf{r}$ in the CuO plane. The CH equation is based on the GL free-energy expansion in terms of this (conserved) order parameter $u$ [23,33,34],

$$f(u) = \tfrac{1}{2}\varepsilon|\nabla u|^2 + V_{GL}(u, T), \qquad (1)$$

where $\varepsilon$ is the parameter that controls the charge modulations and $V_{GL}(u, T) = -\alpha[T_{PS} - T]u^2/2 + B^2u^4/4 + \cdots$ is a double-well potential that characterizes the two (hole-rich and hole-poor) local charge densities of the CDW structure. The phase separation transition temperature $T_{PS}$ is assumed to be near the pseudogap instability at $T^*(p)$.

An elegant way to derive the CH equation is through the continuity equation for the local free-energy current density $\mathbf{J} = M\nabla(\delta f/\delta u)$ [35],

$$\frac{\partial u}{\partial t} = -\nabla \cdot \mathbf{J} = -M\nabla^2[\varepsilon^2\nabla^2 u - \alpha^2(T)u + B^2u^3]. \qquad (2)$$

The equation is nonlinear and solved by a stable and fast finite-difference scheme with free-boundary conditions, and we stop the simulation time $t$ when a given CDW structure is reproduced and the solutions $u(\mathbf{r})$ or $p(\mathbf{r})$ are used in the SC calculations.

We have provided a detailed description of the CH simulations in several previous works [26,27,36]. Figure 1(a) illustrates a typical $V_{GL}(\mathbf{r}, T) \equiv V_{GL}[u(\mathbf{r}), T]$ low-temperature solution for a $p = 0.19$ LSCO compound. We can see that $V_{GL}(\mathbf{r}, T)$ forms an array of side-by-side potential minima that hosts the alternating hole-rich and hole-poor charge density
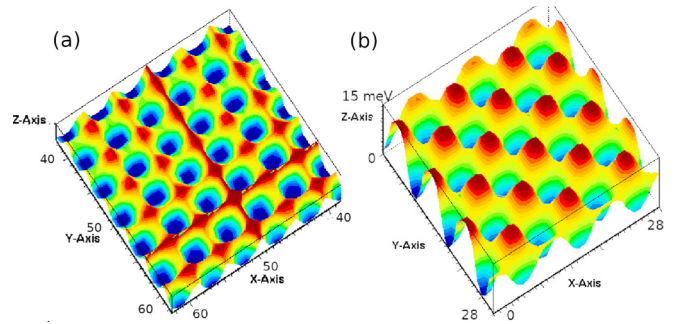


FIG. 1. (a) A three-dimensional plot of the two-dimensional phase separation potential $V_{GL}(\mathbf{r}, T)$ viewed from just above the CuO plane. Notice the array of similar potential wells that host rich and poor alternating charge density domains $p(\mathbf{r})$. (b) Similar view of the SC amplitudes $\Delta_d(\mathbf{r})$ that also follows the same modulation pattern, what is known as pair density waves.

domains (not shown here; see the many simulations in the Supplemental Material of Ref. [27]).

The derived CDW density map that reproduces the measurements of a given compound and the respective $V_{GL}$ will be used in the BdG calculations to obtain the SC properties in the next section.

## III. The BdG SUPERCONDUCTING CALCULATIONS

To perform the BdG SC approach, we use two results from the CH calculations: (1) the CDW density map $p(\mathbf{r})$ and (2) the functional $V_{GL}(\mathbf{r})$ shown in Fig. 1(a).

As mentioned in the Introduction, at low temperatures, $V_{GL}(\mathbf{r}, T)$ constrains the planar charges in alternating hole-rich and hole-poor domains forming the CDW structure. These alternating densities force the ions to oscillate around new displaced positions as observed by x-ray diffraction [37]. They interact back with the holes, leading to a local lattice-mediated hole-hole attraction and Cooper pairs inside the CDW domains, recalling that this is possible because the SC coherence length $\xi$ is in general shorter than $\lambda_{CO}$. This pairing interaction is dependent on the CDW hole-rich and hole-poor local concentrations, and it is reasonable to assume that it scales with the localization potential $V_{GL}(\mathbf{r}, T)$ [26].

We use this interaction as a nearest-neighbor potential attraction in an extended Hubbard model to calculate the local SC amplitudes $\Delta_d(\mathbf{r}_i)$. This is done by a self-consistent approach that keeps the $p(\mathbf{r}_i)$ CDW structure constant from the beginning to the end of the calculations following several different experiments [14–16,22,37]. This is achieved by changing the local chemical potential $\mu(\mathbf{r}_i)$ at each iteration until the $\Delta_d(\mathbf{r}_i)$ amplitudes converge and the density map $p(\mathbf{r}_i)$ is preserved. At the end of the calculations we obtain the original CDW map and the local $d$-wave amplitudes $\Delta_d(\mathbf{r}_i)$ with the same charge modulations $[\lambda_{CO}(p)]$, what is known as pair density waves (PDWs) [25]. This is shown in Fig. 1(b) for the same compound of Fig. 1(a).

The $\Delta_d(\mathbf{r}_i, p, T)$ local spatial variations imply that global properties, such as the condensation energies, critical temperatures, and interlayer-intralayer Josephson coupling, are a

function of the average SC amplitudes [26,27,36] given by

$$\langle \Delta_d(p, T) \rangle = \sum_i^N \Delta_d(\mathbf{r}_i, p, T)/N, \qquad (3)$$

where the sum, as in the case of $\langle V_{GL}(p) \rangle$, is over the $N$ unit cells of a single CuO plane.

## IV. JOSEPHSON COUPLING CALCULATIONS

We mentioned in the Introduction that the CDW structure shown in Fig. 1(a) with its charge domains bounded by the $V_{GL}(\mathbf{r}_i, p, T)$ potential has some similarities with granular materials. In this case, the charges are bounded to the physical grains by the surface potential and local superconductivity may arise in the interior. Long-range order or supercurrents are a consequence of Josephson tunneling between the grains [38]. Although the HTS crystals are not granular in a structural sense, the ubiquitous CDW in these materials led us to suggest [23] that they may form an array of mesoscopic Josephson junctions.

Under this assumption, the SC transition develops in two steps when the temperature decreases [38]: First, the order parameters with local amplitudes $\Delta_d(\mathbf{r}_i, p, T)$ and phases $\theta_i$ arise in each charge CDW domain "$i$." These localized amplitudes give rise to local Josephson coupling $E_J(r_{ij})$ that is proportional to the local supercurrent or the lattice version of the local superfluid density [28] $n_{sc}$, and proportional to the local phase stiffness.

Second, upon further cooling, the local phase stiffness increases and eventually overcomes thermal disorder, which leads to a SC transition by long-range phase order. Therefore, we emphasize that the SC critical temperature $T_c$ is determined by the competition between thermal disorder and the average planar Josephson energy $\langle E_J(p, T) \rangle$.

These in-plane calculations are the fundamental pillars of the three-dimensional long-range-order (LRO) in the whole system, which we infer from transport measurements. For low doping $p$, the $c$-direction resistivity $\rho_c$ is $\approx 10^3$–$10^6$ larger than the $a$- or $b$-axis resistivity $\rho_{ab}$, a behavior shared also by $Bi_2Sr_{2-x}La_xCuO_{6+\delta}$ [39,40]. Despite this huge difference, it is surprising that both $\rho_c(T)$ and $\rho_{ab}(T)$ fall to zero at the same temperature ($T_c$). We have recently argued that the mechanism behind this puzzling behavior may be understood in terms of the planar and weaker out-of-plane average Josephson coupling [23], exactly as the weakly coupled XY models.

As explained previously [24], even for $d$-wave amplitudes, it is sufficient to use the Ambegaokar-Baratoff analytical $s$-wave expression [41] averaged over the plane,

$$\langle E_J(p, T) \rangle^X = \frac{\pi \hbar \langle \Delta_d(p, T) \rangle}{4e^2 R_n^X(p)} \tanh \left[ \frac{\langle \Delta_d(p, T) \rangle}{2k_B T} \right], \qquad (4)$$

where $X = ab$ for planar and $X = c$ for interlayer coupling and $R_n^X(p, \sim T_c)$ is the corresponding normal-state directional resistance just above $T_c$. In our model of an array of Josephson junctions, the current is composed of Cooper pairs tunneling between the CDW domains and by normal carriers or quasiparticle planar current [42]. For a $d$-wave HTS near $T_c$ the supercurrent is dominant [42], which justifies the use of the experimental $R_n(T_c)$ between the charge domains in Eq. (6).

As mentioned, thermal energy causes phase disorder and coherence is achieved [23,36] at $\langle E_J(p, T_c) \rangle^{ab} = k_B T_c$. The smaller planar resistances yield larger $E_J^{ab}$ that promote first LRO in the planes, but each plane $i$ would have its own SC phase $\theta_i$ if it was not for the weaker interplane $E_J^c$ coupling. It is similar to a ferromagnet cooled down in the presence of a tiny magnetic field causing all the moments to become aligned.

Thus, the weaker interlayer coupling $\langle E_J(p, T) \rangle^c$ connects the planes but leads to only a single-phase $\theta$ at $T \leqslant T_c$ in the whole system, and both $c$ and $ab$ resistivity drop off together despite their orders of magnitude difference.

## V. MAGNETIC PENETRATION DEPTH AND RESISTIVITY

According to Eq. (4), due to the large difference in the directional resistivities, we expect smaller superfluid densities $n_{sc}$ along the $c$ direction than along the plane, which is confirmed by the $ab$- and $c$-axis penetration depth anisotropy [7,30,43]. We recall also that the square of the magnetic penetration depth $\lambda$ is inversely proportional to the phase stiffness $\rho_{sc}$ [29] that is proportional to the average Josephson current [28].

Along these lines and in the frame of the LD model [6], Shibauchi et al. [7] successfully reproduced their $c$-axis $\lambda_c(p)$ measurements. We extend here their approach to account for Josephson current between the CDW charge domains in the CuO planes and use that [26,29,36] $\lambda_X^2(p) \propto 1/\langle E_J(p, T) \rangle^X$. Therefore, we may write

$$\left[ \frac{\lambda_c(0)}{\lambda_{ab}(0)} \right]^2 \propto \left[ \frac{\langle E_J(p, T) \rangle^{ab}}{\langle E_J(p, T) \rangle^c} \right] \propto \frac{R_n^c}{R_n^{ab}}, \qquad (5)$$

and $R_n^c = \rho_c(T_c)s$, where $s$, the distance between the CuO layers in double-plane LSCO crystals, is approximately 6.6 Å. This means that $\lambda_c(p)$ is dominated by the interplane Josephson current and, extending this idea, $\lambda_{ab}(p)$ is dominated by the planar average coupling $\langle E_J(p, T_c) \rangle^{ab}$. Therefore, we may write the planar resistivity $R_n^{ab} = \rho_{ab}(T_c)\lambda_{CO}$, since $\lambda_{CO}(p)$ is the distance between the planar CDW domains. Therefore, in a general way,

$$\left[ \frac{\lambda_c(0)}{\lambda_{ab}(0)} \right]^2 \propto \frac{R_n^c}{R_n^{ab}} \propto \frac{\rho_c(T_c)s}{\rho_{ab}(T_c)\lambda_{CO}}. \qquad (6)$$

This expression gives the magnetic penetration depths out of the plane and planar ratio in terms of similar resistivity ratios, the planar distance $s$, and the CDW wavelength $\lambda_{CO}$. Notice that there is not any adjustable parameter in Eq. (6) and all quantities have been measured previously.

Some HTS samples with similar doping have comparable resistivities such as the La- and Y-based compounds studied by Ando et al. [44]. When this is the case the above equation shows why the low-temperature ratios $\lambda_c(p, 0)/\lambda_{ab}(p, 0)$ for different families of compounds have similar values [45]. This is the case for a large number of LSCO and $HgBa_2CuO_{4+x}$ [30] samples and they are also comparable with the measurements of $c$-axis grain-aligned orthorhombic $YBa_2Cu_3O_{7-\delta}$ (YBCO) with $\delta = 0.0, 0.3$, and $0.43$ [46]. The quantitative explanation of these data and their

TABLE I. Data and calculations for LSCO. The first column is the hole density per unit cell. The second is the $[\lambda_c(0)/\lambda_{ab}(0)]^2$ measurements of Shibauchi *et al.* [7] and Panagopoulos *et al.* [30]. The third is the $\rho_c(T_c)/\rho_{ab}(T_c)$ [31,32] resistivity ratios. The fourth is $\lambda_{CO}$ in units of the lattice parameter $a_0 \approx 3.78$ Å measured by RXRD [13]. The last column is the calculations from Eq. (6) with $s = 6.6$ Å that should match the magnetic penetration depth ratio of the second column. For the case of $[\lambda_c(0.09)/\lambda_{ab}(0.09)]^2$, the resistivity data of different groups conflict and we used the $p = 0.10 \pm 0.01$ resistivity ratio $\rho_c/\rho_{ab}$ from Ref. [32] (marked with an asterisk).

| Sample | $[\lambda_c(0)/\lambda_{ab}(0)]^2$ | $\rho_c/\rho_{ab}(T_c)$ | $\lambda_{CO}$ (Å) | $\rho_c s/\rho_{ab}\lambda_{CO}$ |
|---|---|---|---|---|
| $p = 0.09$ | 625 | 2070* | $5.6\,a_0$ | 645* |
| $p = 0.10$ | $\propto 564$ | 1714 | $5.0\,a_0$ | 595 |
| $p = 0.12$ | 441 | 1000 | $4.25\,a_0$ | 408 |
| $p = 0.15$ | 196 | 433 | $3.9\,a_0$ | 193 |
| $p = 0.18$ | 132 | 300 | $3.7\,a_0$ | 164 |
| $p = 0.20$ | 100 | 200 | $3.6\,a_0$ | 97 |

connection with the $\rho_c(T_c)/\rho_{ab}(T_c)$ is one of the main motivations of our present calculations.

On the other hand, most of the data on directional $\lambda_X(0)$ and $\rho_X(T_c)$ with the same doping $p$ were performed a long time ago with LSCO crystals in order to understand the anisotropies in HTS. Nowadays there are single crystals of many other materials, but since the anisotropies are already established, these measurements are not remade. The difficulty to fabricate single crystals in the earlier days of HTS is the reason why data on other materials are practically nonexistent. In most cases, whenever there are data on $\lambda_c(0)/\lambda_{ab}(0)$, they are not accompanied by $\rho_c(T_c)/\rho_{ab}(T_c)$ that is needed by our Eq. (6). Nevertheless, we list in Table I the available data on LSCO for $[\lambda_c(0)/\lambda_{ab}(0)]^2$ [7,30] ratios and $\rho_c(T_c)/\rho_{ab}(T_c)$ [31,32]. For the case of $[\lambda_c(0.09)/\lambda_{ab}(0.09)]^2$, the resistivity data of different groups have discrepant results and we used $\rho_c/\rho_{ab}(0.10 \pm 0.01)$ from Ref. [32] (marked with an asterisk). With these data and the respective CDW wavelengths $\lambda_{CO}(p)$ that enter in Eq. (6) for the planar $R_n^{ab}$, we calculated the magnetic penetration depth ratio. The experimental results and our estimates are plotted together for comparison in Fig. 2, and listed in columns two and five of Table I.

There are also some data on $\lambda_c(0)/\lambda_{ab}(0)$ in the magnetically aligned powder of YBa$_2$Cu$_3$O$_{7-\delta}$ [46] (YBCO) that contains some uncertainty up to 30% in the $c$ axis but provides good estimates of this ratio. Similarly, we use

TABLE II. Data and calculations for optimal YBCO similar to Table I. The uncertainty of 30% in $[\lambda_c(0)/\lambda_{ab}(0)]^2$ is due to the $c$-axis alignment uncertainty of the powders. For YBCO, the distance between two planes is $s = 5.84$ Å and for optimal doping [13] $\lambda_{CO} = 3.12\,a_0$.

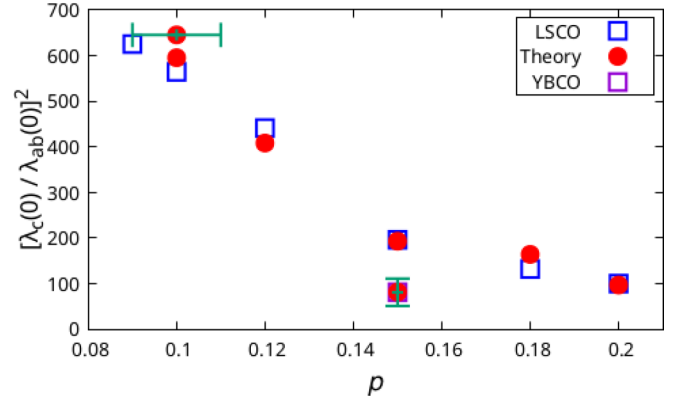| Sample | $[\lambda_c(0)/\lambda_{ab}(0)]^2$ | $\rho_c(T_c)/\rho_{ab}(T_c)$ | $\lambda_{CO}$ (Å) | $\rho_c s/\rho_{ab}\lambda_{CO}$ |
|---|---|---|---|---|
| $p = 0.15$ | $81 \pm 25$ | 167 | $3.9\,a_0$ | 81.5 |



FIG. 2. Six LSCO $[\lambda_c(0)/\lambda_{ab}(0)]^2$ experimental points [7,30] and one optimal YBCO-aligned powder in magnetic field with 30% uncertainty [46] represented by the error bar. They are together with the calculations from Eq. (6) which use the CDW wavelengths [13] $\lambda_{CO}(p)$ and the respective resistivity ratios [31,32] listed in Tables I and II. For $p = 0.09$ we use the resistivities of $p = 0.10 \pm 0.01$ from Ref. [32] as explained in the text.

different anisotropic $\rho_c(T_c)/\rho_{ab}(T_c)$ optimal data on thin films of YBCO grown on an off-axis cut SrTiO3 substrate [47]. Combining these data, we can apply Eq. (6) to this near optimal compound and the calculation is very close to the YBCO experimental result as shown in Fig. 2 and in Table II.

## VI. CONCLUSION

In this paper, we generalize the ideas of ILT and LD models to account also for Josephson coupling between the mesoscopic CDW domains or blocks. The in-plane average Josephson energy is much larger than the interlayer coupling, proportional to $1/\lambda_{ab}^2$ and to the thermal energy at the critical temperature $T_c$. Therefore the SC properties are almost entirely dependent on the planar Josephson coupling in opposition to the old ILT model, which depended on the interlayer Josephson tunneling. Our approach yields values of $\lambda_{ab}$ at least one order of magnitude larger than $\lambda_c$, which gives some insights on why measurements [8] of $\lambda_c$ gave a much smaller condensation energy than the old ILT predictions [5].

Furthermore, we derive an equation relating the magnetic penetration depths $[\lambda_c(0)/\lambda_{ab}(0)]^2$ with the resistivities $[\rho_c(T_c)s]/[\rho_{ab}(T_c)\lambda_{CO}]$ [Eq. (6)], which is in agreement with many measurements without any adjustable parameter. Nowadays there are better single crystals of many materials but since the anisotropies are already established these combined measurements $[\rho_X(T_c)$ and $(\lambda_X(0)]$ on a single sample are no longer explored. However, Eq. (6) provides the motivation for more precise tests in future experiments with modern pristine HTS crystals.

[1] J. R. Clem, Physica C **162-164**, 1137 (1989).

[2] J. R. Clem, Phys. Rev. B **43**, 7837 (1991).

[3] S. Chakravarty, A. Sudbo, P. W. Anderson, and S. Strong, Science **261** 337 (1993).

[4] P. W. Anderson, Science **268**, 1154 (1995).

[5] A. J. Leggett, Science **274**, 587 (1996).

[6] W. Lawrence and S. Doniach, in *Proceedings of the Twelfth International Conference on Low Temperature Physics*, edited by E. Kanda (Academic Press of Japan, Kyoto, 1971), p. 361.

[7] T. Shibauchi, H. Kitano, K. Uchinokura, A. Maeda, T. Kimura, and K. Kishio, Phys. Rev. Lett. **72**, 2263 (1994).

[8] K. A. Moler, J. R. Kirtley, D. G. Hinks, T. W. Li, and M. Xu, Science **279**, 1193 (1998).

[9] P. W. Anderson, Science **279**, 1196 (1998).

[10] J. M. Tranquada, B. J. Sternlieb, J. D. Axe, Y. Nakamura, and S. Uchida, Nature (London) **375**, 561 (1995).

[11] K. M. Lang, V. Madhavan, J. E. Hoffman, E. W. Hudson, H. Eisaki, S. Uchida, and J. C. Davis, Nature (London) **415**, 412 (2002).

[12] O. Fischer, M. Kugler, I. Maggio-Aprile, C. Berthod, and C. Renner, Rev. Mod. Phys. **79**, 353 (2007).

[13] R. Comin and A. Damascelli, Annu. Rev. Condens. Matter Phys. **7**, 369 (2016).

[14] W. D. Wise, M. C. Boyer, K. Chatterjee, T. Kondo, T. Takeuchi, H. Ikuta, Y. Wang, and E. W. Hudson, Nat. Phys. **4**, 696 (2008).

[15] K. K. Gomes, A. N. Pasupathy, A. Pushp, S. Ono, Y. Ando, and A. Yazdani, Nature (London) **447**, 569 (2007).

[16] C. V. Parker, P. Aynajian, E. H. da Silva Neto, A. Pushp, S. Ono, J. Wen, Z. Xu, G. Gu, and A. Yazdani, Nature (London) **468**, 677 (2010).

[17] Y. He, Y. Yin, M. Zech, A. Soumyanarayanan, M. M. Yee, T. Williams, M. C. Boyer, K. Chatterjee, W. D. Wise, I. Zeljkovic, T. Kondo, T. Takeuchi, H. Ikuta, P. Mistark, R. S. Markiewicz, A. Bansil, S. Sachdev, E. W. Hudson, and J. E. Hoffman, Science **344**, 608 (2014).

[18] E. H. da Silva Neto, M. Minola, B. Yu, W. Tabis, M. Bluschke, D. Unruh, H. Suzuki, G. Li, G. Yu, D. Betto, K. Kummer, F. Yakhou, N. B. Brookes, M. Le Tacon, M. Greven, B. Keimer, and A. Damascelli, Phys. Rev. B **98**, 161114(R) (2018).

[19] J. Wu, A. T. Bollinger, X. He, and I. Božović, Nature (London) **547**, 432 (2017).

[20] S.-D. Chen, M. Hashimoto, Y. He, D. Song, K.-J. Xu, J.-F. He, T. P. Devereaux, H. Eisaki, D.-H. Lu, J. Zaanen, and Z.-X. Shen, Science **366**, 1099 (2019).

[21] Y. Fei, Y. Zheng, K. Bu, W. Zhang, Y. Ding, X. Zhou, and Y. Yin, Sci. China: Phys., Mech. Astron. **63**, 227411 (2020).

[22] H. Miao, G. Fabbris, R. J. Koch, D. G. Mazzone, C. S. Nelson, R. Acevedo-Esteves, G. D. Gu, Y. Li, T. Yilimaz, K. Kaznatcheev, E. Vescovo, M. Oda, T. Kurosawa, N. Momono, T. Assefa, I. K. Robinson, E. S. Bozin, J. M. Tranquada, P. D. Johnson, and M. P. M. Dean, npj Quantum Mater. **6**, 31 (2021).

[23] E. V. L. de Mello, Europhys. Lett. **99**, 37003 (2012).

[24] E. V. L. de Mello and J. E. Sonier, J. Phys.: Condens. Matter **26**, 492201 (2014).

[25] E. V. L. de Mello and J. E. Sonier, Phys. Rev. B **95**, 184520 (2017).

[26] E. V. L. de Mello, J. Phys.: Condens. Matter **32**, 40LT02 (2020).

[27] H. S. Santana and E. V. L. de Mello, Phys. Rev. B **105**, 134513 (2022).

[28] B. I. Spivak and S. A. Kivelson, Phys. Rev. B **43**, 3740 (1991).

[29] I. Božović, X. He, J. Wu, and A. T. Bollinger, Nature (London) **536**, 309 (2016).

[30] C. Panagopoulos, J. R. Cooper, T. Xiang, Y. S. Wang, and C. W. Chu, Phys. Rev. B **61**, R3808 (2000).

[31] T. Kimura, K. Kishio, T. Kobayashi, Y. Nakayama, N. Motohira, K. Kitazawa, and K. Yamafuji, Physica C **192**, 247 (1992).

[32] Y. Nakamura and S. Uchida, Phys. Rev. B **47**, 8369 (1993).

[33] E. V. L. de Mello and O. T. da Silveira Filho, Physica A **347**, 429 (2005).

[34] E. V. L. de Mello, R. B. Kasal, and C. A. C. Passos, J. Phys.: Condens. Matter **21**, 235701 (2009).

[35] A. J. Bray, Adv. Phys. **43**, 357 (1994).

[36] E. V. L. de Mello, J. Phys.: Condens. Matter **33**, 145503 (2021).

[37] J. Chang, E. Blackburn, A. T. Holmes, N. B. Christensen, J. Larsen, J. Mesot, R. Liang, D. A. Bonn, W. N. Hardy, A. Watenphul, M. V. Zimmermann, E. M. Forgan, and S. M. Hayden, Nat. Phys. **8**, 871 (2012).

[38] J. B. Ketterson and S. Song, *Superconductivity* (Cambridge University Press, London, 1999).

[39] S. Ono and Y. Ando, Phys. Rev. B **67**, 104512 (2003).

[40] S. Komiya, Y. Ando, X. F. Sun, and A. N. Lavrov, Phys. Rev. B **65**, 214535 (2002).

[41] V. Ambegaokar and A. Baratoff, Phys. Rev. Lett. **10**, 486 (1963).

[42] C. Bruder, A. van Otterlo, and G. T. Zimanyi, Phys. Rev. B **51**, 12904 (1995).

[43] C. Panagopoulos, J. L. Tallon, and T. Xiang, Phys. Rev. B **59**, R6635 (1999).

[44] Y. Ando, S. Komiya, K. Segawa, S. Ono, and Y. Kurita, Phys. Rev. Lett. **93**, 267001 (2004).

[45] T. Schneider and H. Keller, New J. Phys. **6**, 144 (2004).

[46] C. Panagopoulos, J. R. Cooper, and T. Xiang, Phys. Rev. B **57**, 13422 (1998).

[47] G. Heine, W. Lang, R. Rössler, and J. D. Pedarnig, Nanomaterials **11**, 675 (2021).